LAWRENCE
LIVERMORE
NATIONAL
LABORATORY

UCRL-PROC-236273

# Analysis of output surface damage resulting from single 351 nm, 3 ns pulses on sub-nanosecond laser conditioned KD2PO4 crystals

J. Jarboe, J. J. Adams, R. Hackel

November 6, 2007

SPIE - Boulder Damage Symposium
Boulder, CO, United States
September 24, 2007 through September 26, 2007

## Disclaimer

# Analysis of output surface damage resulting from single 351 nm, 3 ns pulses on sub-nanosecond laser conditioned $KD_2PO_4$ crystals

J. A. Jarboe*, J. J. Adams, R. P. Hackel

Lawrence Livermore National Laboratory
7000 East Avenue, L-250
Livermore, CA 94550

**ABSTRACT**

We observe that by conditioning DKDP using 500 ps laser pulses, the bulk damage threshold becomes essentially equivalent to the surface damage threshold. We report here the findings of our study of laser initiated output surface damage on 500 ps laser conditioned DKDP for test pulses at 351 nm, 3 ns. The relation between surface damage density and damaging fluence ($\rho(\phi)$) is presented for the first time and the morphologies of the surface sites are discussed. The results of this study suggest a surface conditioning effect resulting from exposure to 500 ps laser pulses.

Keywords: DKDP, laser-conditioning, surface damage, pulse length, sub-nanosecond laser, damage density

## 1. INTRODUCTION

### 1.1 General

While much work has been done on understanding and mitigating laser-initiated surface damage on fused silica optics [1-3], laser initiated surface damage on $KD_2PO_4$ (DKDP) optics, remains to be studied extensively. One complicating factor in the study of laser-initiated surface damage on DKDP is the relatively-low bulk damage threshold of the material [4] which, in the fluence range of interest, typically results in heavy bulk damage before any surface damage is observed. We have previously reported that 355 nm (3ω), 500 ps pulses are very effective at improving the bulk damage performance of DKDP [4,5]. In fact, we observe that by conditioning DKDP using 500 ps laser pulses, the bulk damage threshold becomes essentially equivalent to the surface damage threshold, making it possible to effectively study surface damage initiated on DKDP at 3w, 3 ns. In this report, we present for the first time surface damage density vs. damaging fluence ($\rho(\phi)$) curves for output surface damage initiated by 3ω, 3 ns pulses and output surface damage probabilities measured at 3ω, 7 ns on 500 ps conditioned DKDP. In general, our results suggest a surface conditioning effect exists due to exposure to the 500 ps pulses. The sizes and morphologies of the surface sites will also be presented and discussed. Note throughout this report we will discuss bulk and surface damage densities and both will be denoted by $\rho(\phi)$. Also, all of the conditioning and damage testing discussed in this report was conducted at a wavelength of either 351 nm or 355 nm and both will be referred to as 3ω throughout.

### 1.2 Review of Bulk Conditioning Using 3ω, 500 ps Laser Pulses

A previous study has shown that 3ω pulse lengths in the 200 – 900 ps range are especially effective at conditioning DKDP against bulk damage initiated at 3ω, 3ns [4]. These studies lead LLNL to the development of a 500 ps conditioning laser [6]. Recent work was performed using this laser to condition a DKDP optic up to various maximum 500 ps conditioning fluences (1, 3, 3.5, 4, and 5 J/cm$^2$) [5]. In that work, damage tests were performed using 3ω, 3ns test pulses to measure the bulk damage density as a function of fluence ($\rho(\phi)$) for the different 500 ps protocols the results of which are summarized in Figure 1. As can be seen, ~2.5X improvement in fluence in $\rho(\phi)$ occurs after conditioning with 500 ps pulses to 5 J/cm$^2$ over unconditioned and the rate of improvement in $\rho(\phi)$ decreases with higher 500 ps

* Correspondence: 925 423-4222, jarboe3@llnl.gov

conditioning fluence. During these experiments, input and output surface damage was also initiated by the 3ω, 3 ns test shots on the DKDP crystal, the analysis of which is the focus of this report.

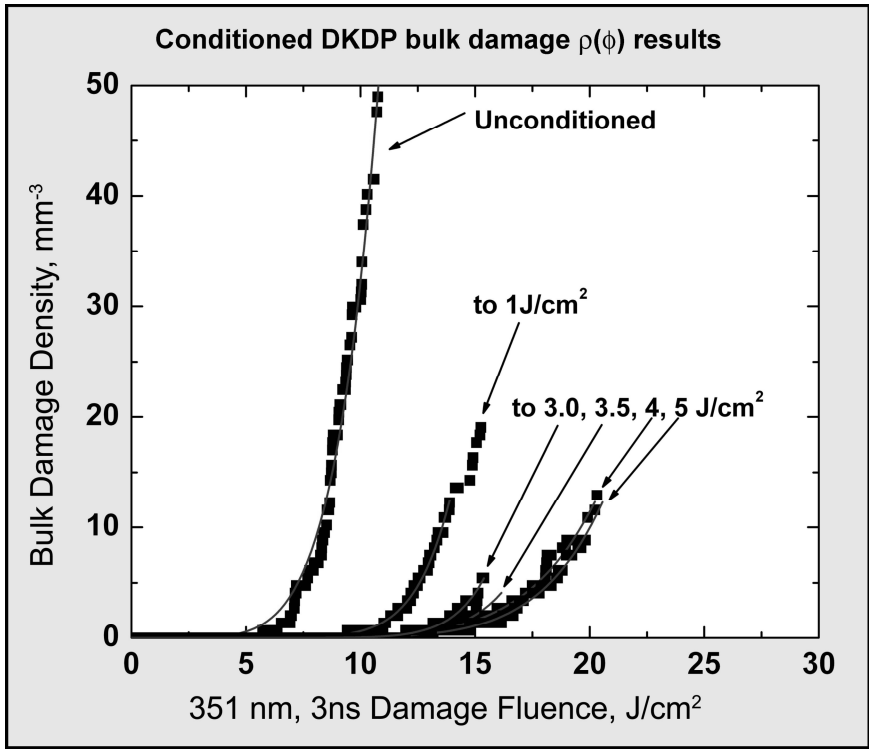


Figure 1: Plot of bulk damage density as a function of fluence (ρ(ϕ)) for 3ω, 3 ns test shots for the various 500 ps conditioning protocols [5]. The labels denote the maximum conditioning fluence used in the protocols. The ρ(ϕ) curve for unconditioned DKDP is shown for comparison. The line through each of the data sets is a numeric fit of a power law of the form $a\phi^b$.

## 2. EXPERIMENTS

### 2.1 Study Goals and Experimental Plans

This study is the output surface damage counterpart of a previous study [5] where the focus was on the bulk damage performance of 500 ps conditioned DKDP. The output surface damage we analyze here was created by the 3 ns test shots used in that previous bulk damage study [5]. Our primary goal here is to measure output surface damage densities as a function of 3ω, 3 ns damaging fluence (ρ(ϕ)) on DKDP conditioned with various 500 ps conditioning protocols. We will systematically study the effect of increasing 500 ps conditioning fluence on surface damage initiated at 3ns using ρ(ϕ) and damage probability measurements. We also examine the morphology of the surface damage sites to determine their size distribution and what percentage, if any, are bulk damage surface eruptions [7].

### 2.2 Conditioning and Test Facilities

#### 2.2.1 The Conditioning Laser

In this section and the next we present for completeness a review of the conditioning and test lasers used in [5]. LLNL developed a 355 nm, 500 ps laser system to take advantage of the optimal conditioning pulse length range. The laser spot size at the conditioning plane is 1.2 mm in diameter. The diameter quoted is the diameter that encompasses 90% of

the energy in the beam. A spatial profile for a typical pulse from the laser can be seen in Figure 2 b.). The beam's spatial profile is nominally a "top-hat" that can be approximated well by a 5$^{th}$-order super-gaussian. Unless otherwise stated, the fluences that will be reported will be the mean value for the fluence over the top 10% of the beam. The circular aperture seen in the figure is for reference and represents a diameter of 1 mm. The beam consistently has a 10% fluence contrast (standard deviation of the mean fluence/mean fluence). The laser operates at a pulse length of 500 ± 15 ps. A typical temporal pulse shape is shown in Figure 2 a.). Temporally, the pulse shape is also nominally "top-hat" and, as shown, has a FWHM of 520 ps that can be fit to a 2$^{nd}$ order super-gaussian.

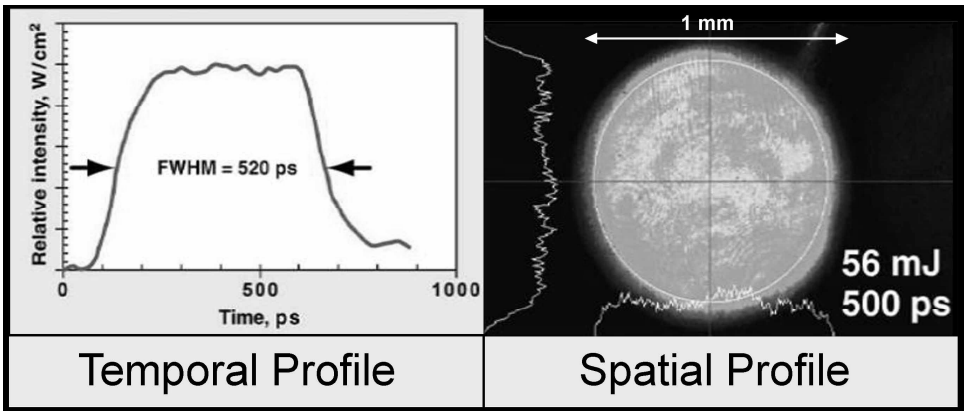


a.) b.)

Figure 2: a.) Typical temporal profile for the sub-nanosecond conditioning laser as measured with the combination of a 45 GHz photo-detector and a sampling oscilloscope. b.) Spatial profile of the sub-nanosecond conditioning beam at the sample plane for a 56 mJ, 500 ps pulse as measured on a CCD. The line-outs at the bottom and left of the image are intensity line-outs spatially along the crosshairs

**2.2.2 Large Area Damage Test Laser**

The 3 ns testing was conducted in the Lawrence Livermore National Laboratory's (LLNL) Optical Sciences Laser (OSL) facility. OSL is a large aperture tripled-Nd:Glass laser with a 10-cm disc amplifier section capable of 180 J at 1053 nm (1ω). The 1053 nm beam is frequency-doubled and tripled using a Type II/Type II conversion scheme with KDP/DKDP crystals. The 351 nm beam is image-relayed from the tripling crystal near to the sample and has a 1/e full-width of 0.9 cm at the sample. The beam's spatial profile is nominally a "top-hat" (as seen in Figure 3b.)) with a somewhat super-gaussian profile across its top 10% and the beam typically has a 12% fluence contrast. OSL also has the capability to operate at a variety of pulse widths and shapes. For these experiments, the temporal pulse shape chosen was nearly gaussian. Figure 3a.) shows a temporal measurement of a nominal 3 ns pulse. Typically, the OSL pulse durations have a ±10% variation from shot-to-shot. The fluences that will be reported will be the mean value for the fluence over the top 10% of the beam. Also, assume all reported fluences for the OSL shots to have an uncertainty of ±12%.

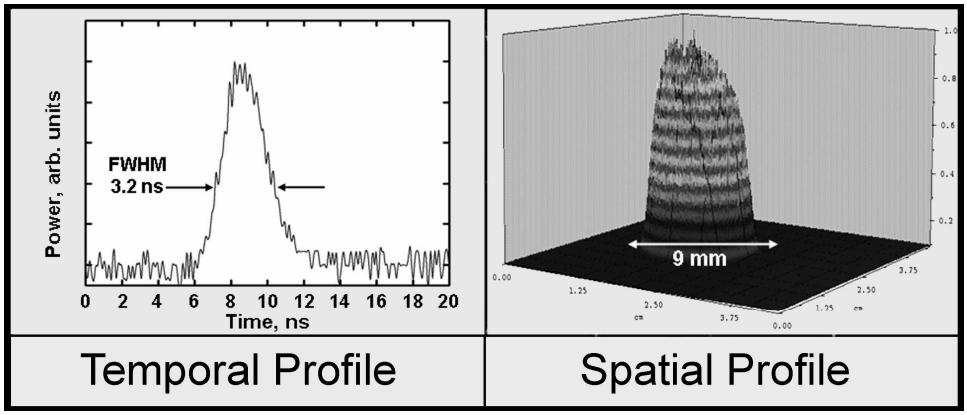


a.) b.)

Figure 3: a.) Typical 3 ns Gaussian temporal profile as measured on a photodiode for a 3ω OSL shot. b.) Spatial profile of the OSL beam at the sample plane for an 8 J/cm$^2$, 3 ns shot at 3ω.

**2.3 Sample Preparation**

The sample used in this experiment was a 15 x 15 x 1-cm$^3$ plate fabricated out of conventional-growth DKDP and oriented for type II mixing of $1\omega + 2\omega \rightarrow 3\omega$. The surfaces of the sample were prepared with a diamond bit-turned finish and were uncoated. The sample was positioned during the experiments so that the direction of the 500 ps conditioning beam's polarization was aligned with the e-axis of the crystal and the input and output surfaces of the crystal during the damage testing were the same as for the conditioning scans.

Pristine regions on the sample were raster-scanned with the 500 ps conditioning laser. The maximum 500 ps conditioning fluences ramped to were 1, 3, 3.5, 4, 5 J/cm$^2$. An appropriate scan overlap and fluence step-size was used. The unconditioned and conditioned regions of the sample which were previously tested with single shots at 3 ns using a 0.9-cm beam [5] were subsequently S/1 and R/1 damage tested at 3ω, 7 ns [8-11]. The S/1 damage test is described in section 3.3 and [8-11]. The entire sample was photographed using a DMS set-up [12-13] which produced a 12-bit digital image of the sample. Figure 4 shows an inverted-contrast DMS image of the DKDP crystal after the conditioning scans, the single-shot damage testing at 3 ns, and the S/1 and R/1 damage testing at 7 ns. In a previous report [5] we discussed in detail the 3 ns damage testing, the results of which were reviewed in section 1.2. The arrays of sites tested in the S/1 and R/1 testing are labeled. The individual highly scattering sites appearing in the arrays, especially in the 1, 3.5, and 5 J/cm$^2$ conditioned regions is surface damage resulting from the S/1 and R/1 testing. The regular horizontal white stripes along the right edge of the part are scatter from vacuum chuck marks [12]. The part shows a variety of small scatter sites over its surface primarily arising from surface particles and damage resulting from handling the crystal. The bright spot in the image at approximately the 8 o'clock position on the crystal is scatter from a large pre-existing surface site.

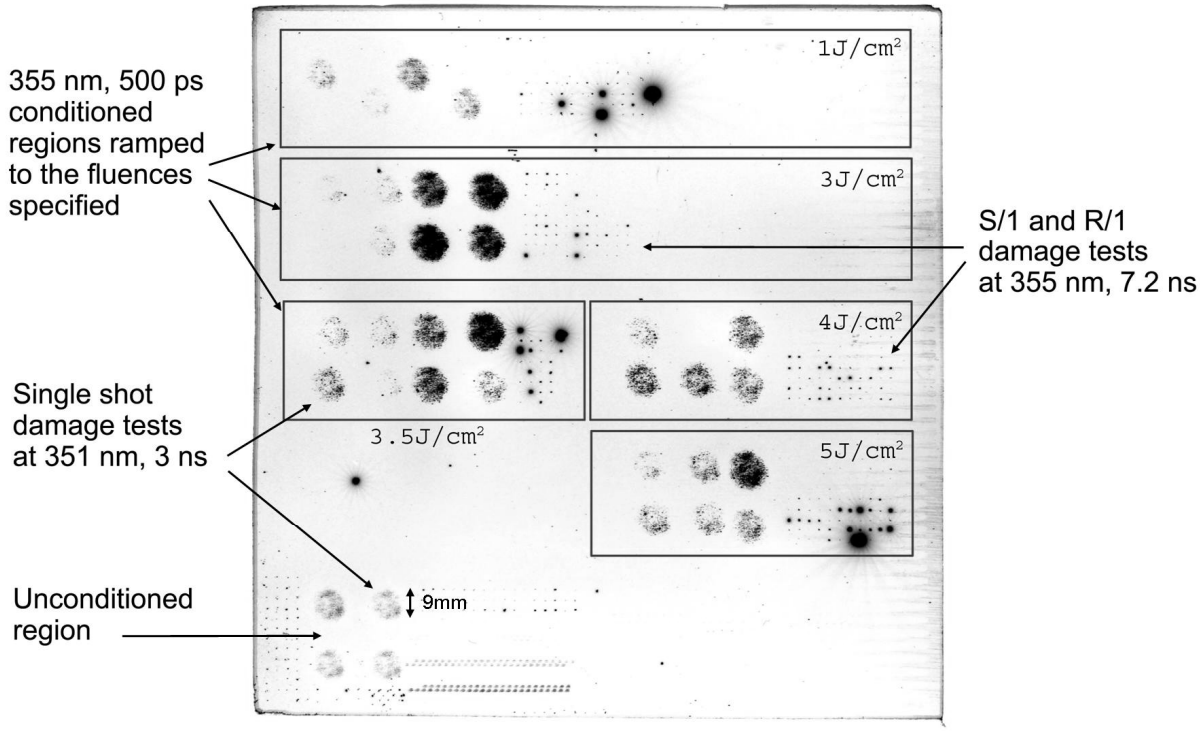


Figure 4: Inverted contrast 12-bit electronic image of the DKDP crystal taken on a DMS [12-13] after the conditioning scans and damage testing. The OSL beam diameter used for the 3 ns testing was 9 mm as denoted in the figure. The clear aperture of the 15 cm part shown is 135 x 135 $mm^2$. The boxes denote the approximate regions ramp-conditioned with the 500 ps laser and the fluence labels denote the maximum conditioning fluence used for each of the protocols. The array of scatter sites resulting from the S/1 and R/1 damage testing [8-11] in each of the regions are as labeled.

**2.4 Measuring Surface Damage Density as a Function of Fluence, ρ(ϕ)**

Figure 5 illustrates the process in which ρ(ϕ) measurements are extracted from a damaged area on a crystal [14]. The basic procedure for measuring output surface ρ(ϕ) is to damage the surface of the crystal while recording a calibrated spatial profile of the damaging beam. The spatial profile is used to determine the damaging beam's fluence distribution over the beam. The next step is to extract the output surface damage data from the crystal. The optic is side illuminated and a scatter image is generated by taking a photograph. The scatter image is then used to determine coordinates that an automated-scanning optical microscope can use to scan the appropriate area on the crystal's surface. The microscope locates and sizes the surface damage sites over the damaged region of interest. The microscope and fluence data is then binned into 700 x 700 $\mu m^2$ bins. The binned densities and fluence data are then independently ordered from low to high, and combined to construct an ordered-ρ(ϕ) curve which will be referred to as simply ρ(ϕ).

It was determined that plotting the ρ(ϕ) data as ordered pairs (rather than x-y registered) produces a smooth well-behaved curve through the center of the noise in the x-y registered data. In other words, the ordered plot of the data is very close to a numerical "best-fit" to the x-y registered data. The ordering is carried out by first sorting the binned fluence data from lowest to highest value independent of the damage site data and then sorting the binned site data similarly. Then the two sorted sets of data are put into one-to-one correspondence and plotted as shown in Figure 5. For

the current work, this technique may be considered the equivalent of ensemble smoothing the data (which yields similar results). We believe the ordered pairs plot is a sensible way to present the ρ(ϕ) data if the damage density is an increasing function of the fluence and the majority of the error sources are random.

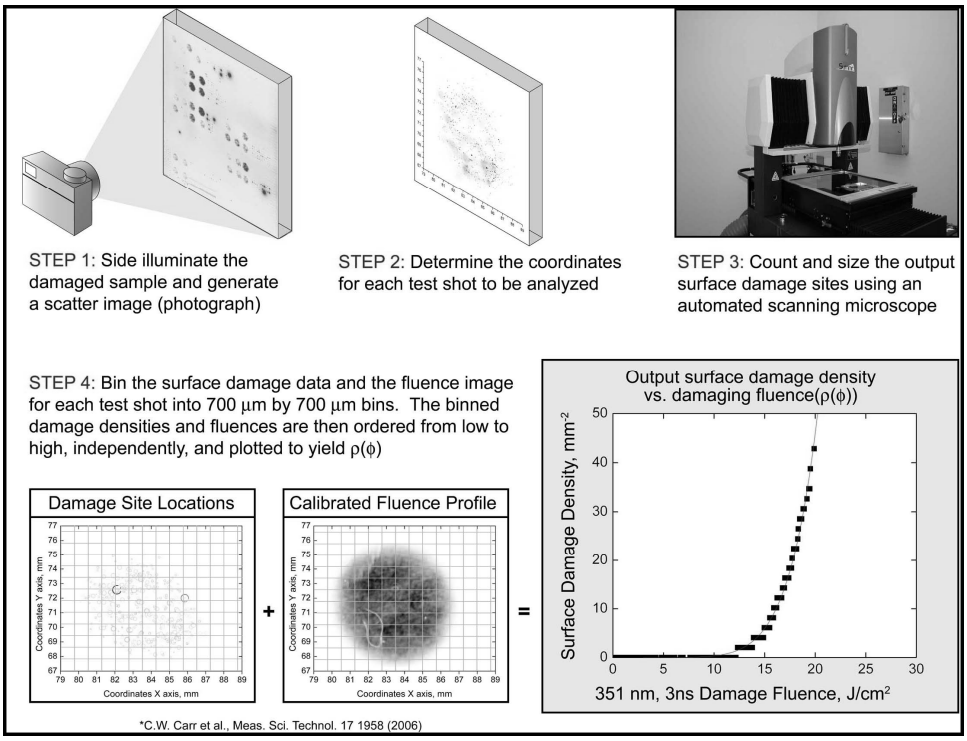


Figure 5: Process steps to extract surface ρ(ϕ) measurements from a damaged area on the sample and the corresponding damaging beam's fluence spatial profile. The total number and spatial distribution of the surface damage sites are determined using an automated-scanning optical microscope. The density and fluence data are binned, independently ordered from low to high, and combined [4,14] to construct the ρ(ϕ) curves presented.

## 3. RESULTS AND DISCUSSION

### 3.1 Output Surface ρ(ϕ) vs. 500 ps Conditioning Protocol

Analysis of the output surface damage resulting from select 3 ns test shots on each of the different conditioned regions on the crystal was performed as described in section 2.4. Figure 6 shows the measured output surface ρ(ϕ) vs. 3 ns test fluence curves for the various 500 ps conditioned regions. Note we were successful at measuring output surface ρ(ϕ) for each of the five 500 ps conditioning protocols, however due to a lack of surface damage we were not able to measure a surface ρ(ϕ) for the shots on the unconditioned region. Because of our choice of 700 x 700 $\mu m^2$ bins the minimum resolvable surface damage density is 2 $mm^{-2}$. Also, the multiple fluences that appear for a given density, for instance, in the 5 $J/cm^2$ results we believe is an artifact of our bin size and method of averaging that we plan to investigate in future work. Determining the output surface ρ(ϕ) curves for the various 500 ps conditioned regions allows us to quantitatively evaluate if there is any apparent effect due to increasing 500 ps conditioning fluence, i.e. if there is any surface "conditioning" effect. The data shows that the $5J/cm^2$ conditioning protocol produced a distinct shift in the surface damage ρ(ϕ) to higher fluence over the other protocols. The typical error in the fluence (±15%) measurement (error bars shown) adds uncertainty to the magnitude of this shift. Further investigation using higher conditioning fluences coupled with higher damage test fluence may help to clarify the apparent shift in the surface damage ρ(ϕ).

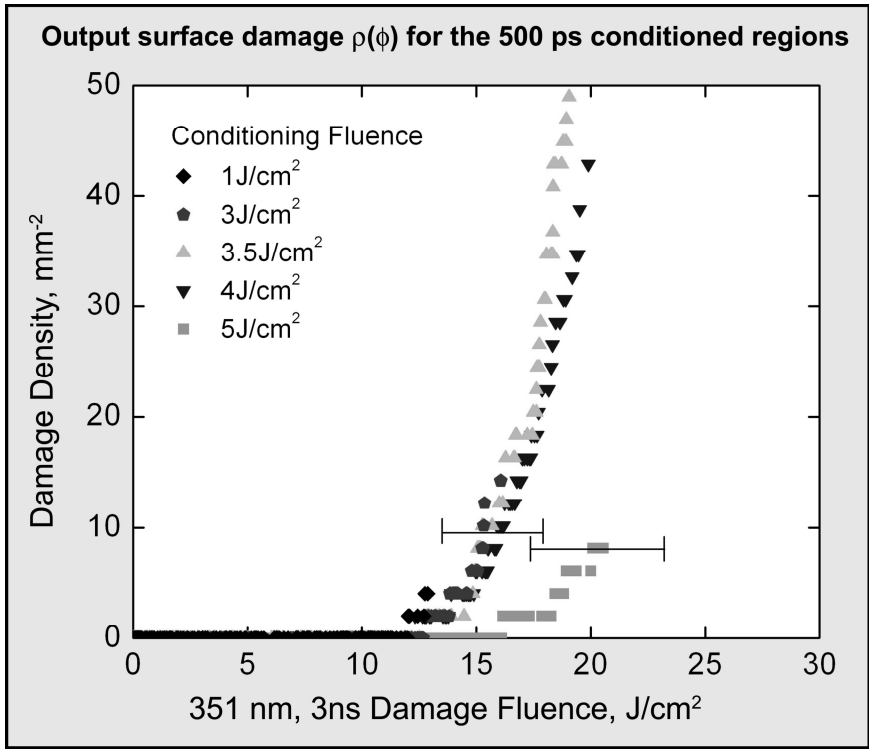


Figure 6: Plot of output surface damage density vs. 3ω, 3 ns test fluence (ρ(ϕ)) for the different 500 ps conditioning protocols determined using the analysis discussed in section 2.4. Note the apparent shift in the surface damage ρ(ϕ) to higher fluence for the 5J/cm$^2$ conditioning protocol.

### 3.2 Total Number of Output Surface Sites Initiated at 3ω, 3 ns vs. 500 ps Conditioning Protocol

In the last section we discussed the output surface damage initiated by the 3ω, 3 ns test shots in terms of ρ(ϕ). There we believe that a surface conditioning effect was observed due to the 5 J/cm$^2$ protocol though there was some uncertainty to this conclusion. Another measure of the output surface damage created by the 3ω, 3ns test shots is the total number of surface sites initiated over the area of the test beam. This is a more basic measurement for the surface damage initiated as opposed to ρ(ϕ) however it may help to clarify the possibility of a surface conditioning effect. Figure 7 plots the total number of output surface damage sites resulting from select 3ω, 3 ns test shots on the 3, 4, and 5 J/cm$^2$ 500 ps conditioned regions. The shots selected for the plot have similar mean fluences (15.0 ± 0.5 J/cm$^2$) and beam fluence contrast (12%). In order to make an appropriate relative comparison, test shots with similar mean fluences were selected to reduce differences in the number of sites initiated due to fluence differences in the shots. The uncertainty in the measurement of the total number of surface sites is ~±5% due primarily to variation in the detection sensitivity of the automated microscope between the different areas analyzed. As can be seen in Figure 7, there is over an order of magnitude decrease in the total number of surface sites created on the 5 J/cm$^2$ protocol as compared to the 3 J/cm$^2$ protocol. In fact, the plot shows there is a systematic decrease in the number of surface sites initiated as the conditioning fluence increases. For example, between the 3 and 4 J/cm$^2$ protocols there is an ~3X decrease in the number of sites initiated and between the 4 and 5 J/cm$^2$ protocols there is a factor of ~8X decrease. We interpret this systematic decrease in the total number of output surface sites initiated with increasing conditioning fluence as a surface "conditioning" effect due to the 500 ps exposure. Note this is the same conclusion drawn less conclusively in the previous section.

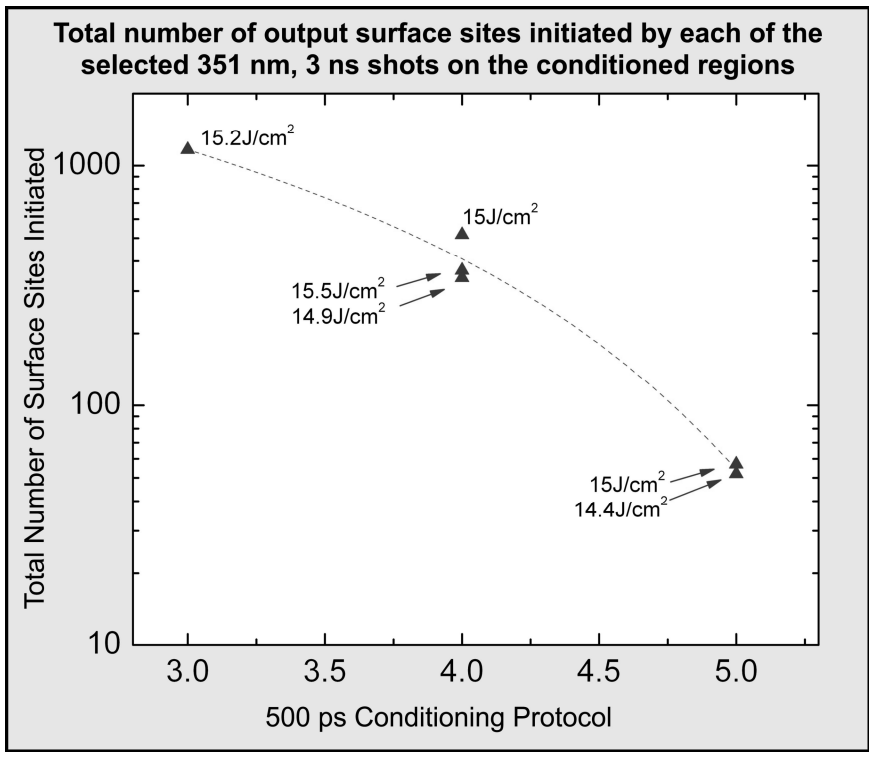


Figure 7: Total number of output surface sites created by selected 3ω, 3 ns test shots on the 3, 4, and 5 J/cm$^2$ 500 ps conditioning protocols. The 3 ns test shots selected have similar mean fluences (15 ± 0.5 J/cm$^2$) and beam fluence contrast (12%). The uncertainty in the measurement of the total number of surface sites is ~±5%. Note the test shots on the 5 J/cm$^2$ protocol had over an order of magnitude decrease in the total number of output surface sites initiated as compared to the number sites initiated on the 3 J/cm$^2$ protocol.

**3.3 Output Surface Damage Probability vs. 500 ps Conditioning Protocol**

3ω, 7 ns S/1 and R/1 bulk damage tests [8-11] were conducted on the various 500 ps conditioned regions of the crystal to independently evaluate the conditioning effectiveness and for comparison to the bulk ρ(ϕ) results presented previously [5,8]. These experiments were conducted with a small beam (650 μm) as opposed to the relatively large beam (10 mm) used for the ρ(ϕ) testing. During this 3ω damage probability testing *both* bulk and surface damage was initiated in each of the sites again implying that the bulk and surface damage thresholds are essentially equivalent after the 500 ps conditioning. Output surface damage probabilities measured at the same fluence (28 J/cm$^2$) were determined for the 3.5, 4, and 5 J/cm$^2$ conditioned regions as shown in Figure 8. The 3.5 and 4 J/cm$^2$ protocols had the same probability (40%) for output surface damage, however, within the experimental error; we see a decrease in the probability for surface damage between conditioning to 4J/cm$^2$ and 5J/cm$^2$, again supporting a surface conditioning effect. At this point we can only speculate on a possible physical origin of this surface conditioning effect. In general, we believe that precursors either at or very near (within ~1μm) the surface are being removed or modified (conditioned) by the 500 ps exposure that increases their damage threshold and leads to the conditioning effect observed here.

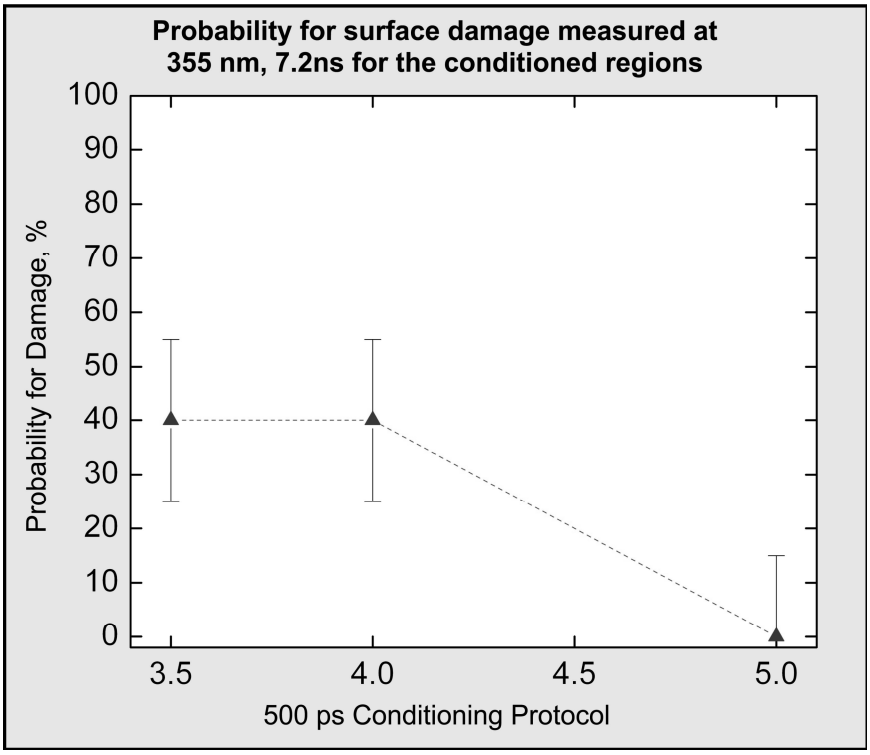


Figure 8: Plot of output surface damage probabilities for the 3.5, 4, and 5 J/cm$^2$ 500 ps conditioning protocols. The damage probabilities were measured at 3ω, 7 ns in an S/1 [8-11] fashion using a single fluence of 28 J/cm$^2$. Note the significant decrease in the output surface damage probability between the 4 J/cm$^2$ and 5 J/cm$^2$ conditioning protocols.

**3.4 Morphology and Size Distribution for the Output Surface Damage Sites Initiated at 3ω, 3ns**

In this section, we examine the morphology of the surface damage sites initiated by one of the test shots using high resolution (maximum of 0.136 μm/pixel) optical microscopy in order to determine their distribution of sizes and what percentage, if any, are bulk damage surface eruptions [7]. The region examined was the 9 mm diameter area illuminated by the 15 J/cm$^2$ test shot on the 4 J/cm$^2$ 500 ps conditioned region. All of surface damage sites that could be resolved within the 9 mm diameter area were photographed, sized, and classified according to morphology. A total of 1550 sites were photographed. We determine four distinct output surface damage morphologies. Figure 9 shows representative micrographs of the four distinct morphologies. The four distinct morphologies are referred to as "Pits", "Chips", "Partial" bulk damage surface eruptions, and "Full" bulk damage surface eruptions.

We believe the "Pits" and "Chips" are damages from precursors native to the surface (non bulk damage related) whereas the "Partial" and "Full" morphologies are damages resulting from the initiation of bulk damage near the surface either partially breaking through the surface as shown on the lower left or completely breaking through leaving the distinct crater shown on the lower right. In the example micrograph of the "Full", we can see a typical bulk damage surface eruption. The 5 μm bulk damage core [2,5] can be seen at the center of the crater with the surrounding radially propagating crack structure both of which are distinct of a bulk damage surface eruption [7]. The "Pits" are very similar to grey haze [2, 15] initiated on fused silica surfaces due to their small diameter (~1 μm) and apparent circular shape and the "Chips", too, are very similar in morphology to typical surface damage initiated on fused silica in the 30 μm range [1-3].

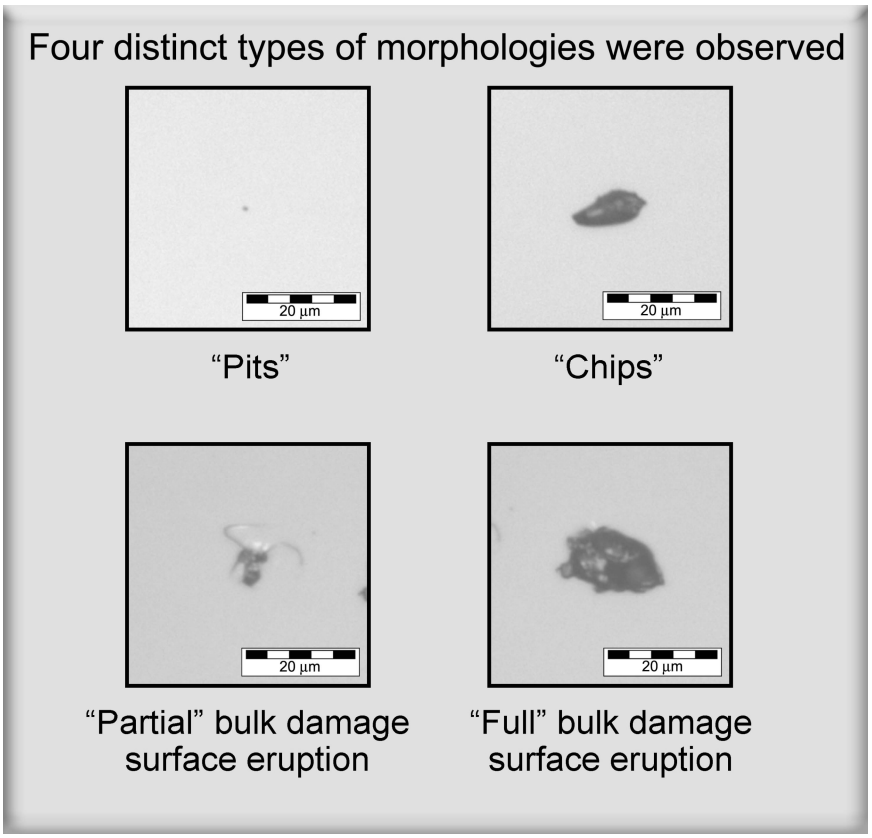


Figure 9: Examples of the four distinct output surface damage morphologies initiated by the 15 J/cm$^2$ test shot on the 4 J/cm$^2$ 500 ps conditioned region of the crystal. The micrographs were collected using high resolution microscopy (0.136 µm/pixel). The four distinct morphologies are referred to as "Pits", "Chips", "Partial" bulk damage surface eruptions, and "Full" bulk damage surface eruptions. In the "Full" micrograph on the lower right, the 5 µm bulk damage core can be seen at the center of the crater with the surrounding radially propagating crack structure both of which are distinct of a bulk damage surface eruption [7].

Figure 10 shows the mean diameter distributions for the four distinct morphologies of surface damage sites. The sites are grouped into two major categories: non-eruptions ("Pits" and "Chips") and bulk eruptions ("Partial" and "Full") based on the discussion above. The "Pits" have a size distribution of 2 ± 1 µm and account for ~40% of the total sites. These "Pits" were randomly distributed over the area of the beam and because of their small size were not detected in the $\rho(\phi)$ analysis. The resolution used in the $\rho(\phi)$ analysis was 1.2 µm/pixel. We do not feel that this has any impact on the accuracy of the $\rho(\phi)$ curves or on the conclusions drawn in the previous sections but it is the subject of future work. The "Chips" have a size distribution of 3 – 17 µm with the majority of the sizes falling in the 3 – 10 µm range. The "Chips" account for ~55% of the total sites. Combined, the non-eruptions account for ~98% of the total sites measured.

For the bulk eruptions category, we counted 33 "Partial" and three "Full" bulk damage surface eruptions. The "Partials" have a size distribution that ranges from 6 to 17 µm as can be seen in Figure 10 and accounts for 2% of the total sites. Only three sites were classified as "Full" bulk damage surface eruptions, which is less than 1% of the total sites counted. In total, bulk eruptions accounted for only ~2% of the total sites measured. The 33 "Partial" and three "Full" bulk eruptions were included in our $\rho(\phi)$ analysis which we estimate contributes to less then 5% of the sites used for that analysis. Based on this, we believe bulk damage surface eruptions are not a significant factor in our $\rho(\phi)$ analysis implying that the surface conditioning effect we observe is purely surface related.

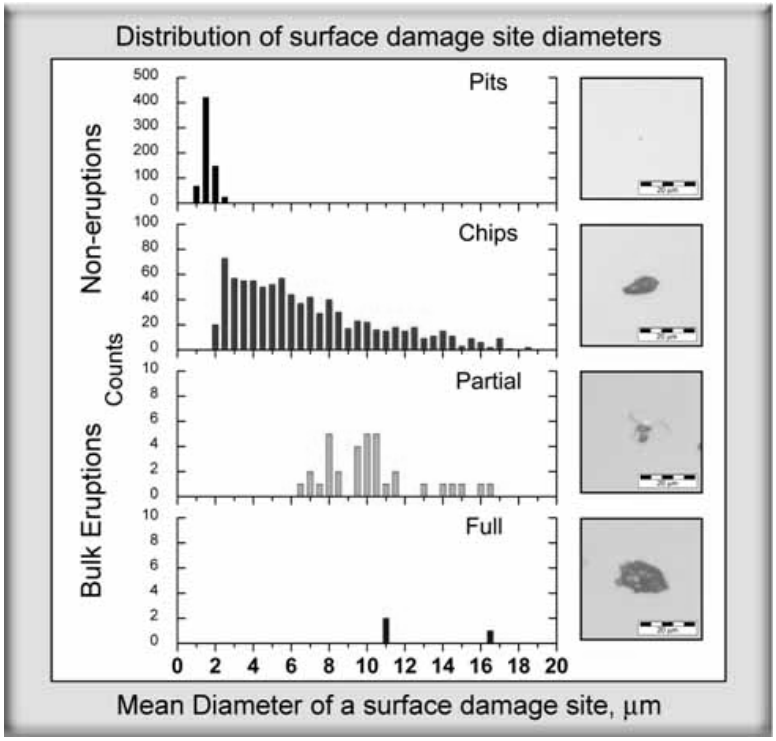


Figure 10: Mean diameter distributions for the four distinct morphologies of surface damage sites initiated by a 15 J/cm$^2$ pulse (3ω, 3ns) on 500 ps conditioned DKDP. The sites are grouped into two major categories: non-eruptions ("Pits" and "Chips") and bulk eruptions ("Partial" and "Full"). The diameters measured for the various morphologies in general ranges from 1-20 μm. Note the bulk eruptions ("Partial" and "Full") account for only ~2% of the total sites.

## 4. SUMMARY

This study was the surface damage counterpart to a previous study [5] discussing the effectiveness of 3ω, 500 ps laser pulses at conditioning DKDP against bulk damage. We observe that 3ω, 500 ps laser conditioning of DKDP can raise the bulk damage threshold to be essentially equivalent to the surface damage threshold. We successively measured, for the first time, output surface damage density vs. 3ω, 3ns damaging fluence ($\rho(\phi)$) curves for 500 ps conditioned DKDP. Surface damage $\rho(\phi)$ curves were determined for five different 500 ps conditioning protocols.. A distinct shift in the data to higher fluence was observed for the 5 J/cm$^2$ protocol but due to the error bars, there is uncertainty in the magnitude of this shift. When the total number of output surface sites initiated per 3ω, 3 ns test shot on the different 500 ps conditioning protocols was compared, we observe more than an order of magnitude decrease in the total number of surface sites initiated between the 3 and 5 Jcm$^2$ conditioning protocols. Results from an independent small beam surface damage probability test also indicated a surface conditioning effect when conditioning above 4 J/cm$^2$, 500 ps. We presented three different sets of measurements that support the conclusion that a surface conditioning effect occurs in DKDP due to exposure to 500 ps pulses. High resolution microscopy was performed on surface damage resulting from a 15 J/cm$^2$ test shot on the 4 J/cm$^2$ conditioned region. We classified four distinct output surface damage morphologies and size distributions were reported for each. We estimate that bulk damage surface eruptions represent between 2-5% of the total surface damage sites measured. Therefore, we believe bulk damage surface eruptions are not a significant factor in our $\rho(\phi)$ analysis suggesting that the surface conditioning effect we observe is purely surface related.

## REFERENCES


1. M. A. Norton, E. E. Donohue, M. D. Feit, R. P. Hackel, W. G. Hollingsworth, A. M. Rubenchik, and M. L. Spaeth, " Growth of laser damage on the input surface of $SiO_2$ at 351 nm," 2006 SPIE Proceedings, **6403**, 64030L-2 (2007)
2. C. W. Carr, M. J. Matthews, J. D. Bude, and M. L. Spaeth, "The effect of laser pulse duration on laser-induced damage in KDP and $SiO_2$," 2006 SPIE Proceedings, **6403**, 64030K-1 (2007)
3. L. Gallais, J. Capoulade, F. Wagner, H. Krol, J.-Y. Natoli, M. Commandre, S. Kurbanov, "Luminescence, absorption and morphology studies of laser-damage sites in silica glasses and coatings," 2005 SPIE Proceedings, **5991**, 59910A-1 (2006)
4. J. J. Adams, T. L. Weiland, J. R. Stanley, W. D. Sell, R. L. Luthi, J. L. Vickers, C. W. Carr, M. D. Feit, A. M. Rubenchik, M. L. Spaeth, R. P. Hackel, "Pulse length dependence of laser conditioning and bulk damage in $KD_2PO_4$," 2004 SPIE Proceedings, **5647**, 265 (2005)
5. J. J. Adams, J. A. Jarboe, C. W. Carr, M. D. Feit, R. P. Hackel, J. M. Halpin, J. Honig, L. A. Lane, R. L. Luthi, J. E. Peterson, D. L. Ravizza, F. Ravizza, A. M. Rubenchik, W. D. Sell, J. L. Vickers, T. L. Weiland, T. J. Wennberg, D. A. Willard, M. F. Yeoman, "Results of sub-nanosecond laser-conditioning of $KD_2PO_4$ crystals," 2006 SPIE Proceedings, **6403**, 64031M-1 (2007)
6. J. Honig et al. to be submitted
7. W. C. Carr, personal communication, LLNL
8. J. J. Adams, J. A. Jarboe, M. D. Feit, R. P. Hackel, "Comparison between S/1 and R/1 tests and damage density vs. fluence ($\rho(\phi)$) results for unconditioned and sub-nanosecond laser-conditioned $KD_2PO_4$ crystals," *these proceedings*, paper number 6720-53
9. M. Runkel and M. Nostrand, "An overview of raster scanning for ICF-class laser optics," 2002 SPIE Proceedings, **4932**, 136 (2003)
10. A. K. Burnham, M. Runkel, R. A. Hawley-Fedder, M. L. Carman, R. A. Torres, and P. K. Whitman, "Low-temperature growth of DKDP for improving laser-induced damage resistance at 350 nm," 2000 SPIE Proceedings, **4347**, 373 (2001)
11. R. Sharpe and M. Runkel, "Automated damage onset analysis techniques applied to KDP damage and the Zeus small area damage test facility," 1999 SPIE Proceedings, **3902**, 361 (2000)
12. M. Runkel, J. Bruere, W. Sell, T. Weiland, D. Milam, D. Hahn, M. Nostrand, "Effects of pulse duration on bulk laser damage in 350-nm raster scanned DKDP," 2002 SPIE Proceedings, **4932**, 405 (2003)
13. F. Rainer, "Mapping and inspection of damage and artifacts in large-scale optics," 1996 SPIE Proceedings, **3244**, 272 (1997)
14. C. W. Carr, M. D. Feit, M. C. Nostrand, and J. J. Adams, "Techniques for qualitative and quantitative measurement of aspects of laser-induced damage important for laser beam propagation," Meas. Sci. Technol., **17**, 1 (2006)
15. J. Yoshiyama, F. Y. Genin, A. Salleo, I. Thomas, M. R. Kozlowski, L. M. Sheehan, I. D. Hutcheon, and D. W. Camp, "A study of the effects of polishing, etching, cleaving, and water leaching on the UV laser damage of fused silica," 1997 SPIE Proceedings, **3244**, 331 (1998)


This work performed under the auspices of the U.S. Department of Energy by Lawrence Livermore National Laboratory under Contract DE-AC52-07NA27344. UCRL-PROC-236273